# Hydrogen Release from Sodium Alanate Observed by Time-resolved Neutron Backscattering

#### Aline Léon

Karlsruhe Institute of Technology, Institute of Nanotechnology, Hermann-von-Helmholtz-Platz 1, 76344 Eggenstein-Leopoldshafen, Germany\*

## Joachim Wuttke

Jülich Centre for Neutron Science JCNS, Forschungszentrum Jülich GmbH, Outstation at FRM II, Lichtenbergstr. 1, 85747 Garching, Germany<sup>†</sup> (Dated: June 8, 2019)

Innermolecular motion in Na<sub>3</sub>AlH<sub>6</sub> gives rise to a Lorentzian spectrum with a wavenumber-independent width of about 1  $\mu$ eV at 180°C, which is probably due to rotation of AlH<sub>6</sub> tetrahedra. There is no such quasielastic line in NaAlH<sub>4</sub> or NaH. Based on this finding, time-resolved measurements on the neutron backscattering spectrometer SPHERES were used to monitor the decomposition kinetics of sodium alanate, NaAlH<sub>4</sub>  $\rightarrow$  Na<sub>3</sub>AlH<sub>6</sub>  $\rightarrow$  NaH. Both reaction steps were found to be accelerated by autocatalysis, most likely at the surfaces of Na<sub>3</sub>AlH<sub>6</sub> and NaH crystallites.

## PACS numbers: 88.30.R-,82.30.Lp,63.50.-x,61.05.F-

## I. INTRODUCTION

Sodium alanate NaAlH<sub>4</sub> is widely studied as a model system for hydrogen storage [1–3]. While hydrogen exchange in pure bulk alanate is not reversible, hydrogen desorption and absorption kinetics has been improved decisively by doping [4, 5] and nanostructuring [6–8]. Further improvement of the hydriding/dehydriding kinetics requires a detailed understanding of the reaction mechanism.

In this work, we introduce time-resolved neutron backscattering as a new tool to monitor the solid-state reactions that are responsible for hydrogen release. Measurements are carried out on pure NaAlH<sub>4</sub> and its decomposition products Na<sub>3</sub>AlH<sub>6</sub> and NaH; one explorative experiment has been undertaken on material doped with TiCl<sub>3</sub>, cycled under hydrogen, and quenched in the hydrogenated state.

## A. The Hydriding/Dehydriding Reactions

Hydrogen storage in sodium alanate is based on the two reactions

$$NaAlH_4 \leftrightarrow \frac{1}{3}Na_3AlH_6 + \frac{2}{3}Al + H_2,$$
 (1)

$$Na_3AlH_6 \leftrightarrow 3NaH + Al + \frac{3}{2}H_2.$$
 (2)

A third reaction, the decomposition of NaH, has no practical importance, because it only occurs above  $425^{\circ}$ C [9]. Therefore, a theoretically reversible capacity of 5.6 wt.% hydrogen is available. The equilibrium temperatures of

\*Electronic address: aline.leon@kit.edu †Electronic address: j.wuttke@fz-juelich.de

(1) and (2) depend only little on doping, but much on pressure [10]. At 1 bar, they are about  $30^{\circ}\mathrm{C}$  and  $110^{\circ}\mathrm{C}$ , respectively, with uncertainties of several degrees [11, Fig. 2]. A thermodynamic argument suggests that at particle sizes below 50 nm, NaAlH<sub>4</sub> may decompose in a single step into NaH, Al, and H<sub>2</sub> [12]. On the other hand, time-resolved neutron diffraction during hydrogen release from NaAlH<sub>4</sub> with a particle size of 110 nm clearly shows a transitory state rich in Na<sub>3</sub>AlH<sub>6</sub> [13].

In undoped bulk NaAlH<sub>4</sub>, reaction rates for hydrogen release are very low, unless the temperature approaches the melting point for which values between 175°C and 190°C are reported [13–16]. In pure ball-milled NaAlH<sub>4</sub> at 170°, it takes at least 8 h to complete the desorption step (1). When doped with Ti clusters, for example, this step takes only 300 s at 150°C [16].

From studies on doped material, it can be concluded that the reactions (1), (2) take place at the boundary between Al particles and NaH, Na<sub>3</sub>AlH<sub>6</sub>, or NaAlH<sub>4</sub> phases [17] and that the rates of these reactions are limited by a nucleation/growth process [18] or/and by the transport of heavy, Al- or/and Na-based species [1, 19]. This is supported by H/D exchange experiments showing that the rate-limiting step of the hydriding/dehydriding process is neither H<sub>2</sub> dissociation nor H diffusion [20, 21].

Quite different mechanisms have been proposed to explain the effect of titanium doping: (i) Ti is a surface catalyst [20, 22–24]; (ii) Ti creates  $\mathrm{Na^+}$  vacancies in the bulk structure, thereby facilitating hydrogen diffusion [13, 25, 26] or/and the transport of heavier species [13, 19]; (iii) Ti weakens the Al-H bond, promoting the removal of  $\mathrm{H_2}$  [27]; (iv) TiCl<sub>3</sub> is a grain refiner preventing growth of Al and NaH particles [13]; (v) Ti is an initiator of Al nucleation [24].

## B. Quasielastic Neutron Scattering Studies

We are aware of two previous quasielastic neutron scattering measurements. One measurement using a tripleaxis spectrometer on NaAlH<sub>4</sub> at 150°C indicates that a small fraction (< 10%) of H atoms participates in a fast localized process (almost q independent Lorentzian halfwidth  $\Gamma \simeq 70 \ \mu eV$ , corresponding to a characteristic time of  $\tau = \hbar/\Gamma \simeq 10$  ps) [28]. Doped and undoped NaAlH<sub>4</sub> and Na<sub>3</sub>AlH<sub>6</sub> were investigated using the Jülich backscattering spectrometer BSS [29, 30]. In doped NaAlH<sub>4</sub> at 117°C, about 0.5% of the hydrogen were found to be mobile, too little to make reliable statements about its motion [29]. In doped Na<sub>3</sub>AlH<sub>6</sub> at 77°C and in undoped NaAlH<sub>4</sub> at 117°C, some quasielastic broadening was observed although the Lorentzian width  $\Gamma$  was considerably smaller than the resolution fwhm of 0.8  $\mu$ eV [30]. As no spectral fits were shown, it is not possible to assess the conclusion of broadening being due to jump diffusion.

In the meantime, Forschungszentrum Jülich has replaced the BSS by the new backscattering spectrometer SPHERES [31]. Compared to BSS, SPHERES has much higher count rates, better resolution (0.65  $\mu eV$ ), a wider dynamic range, and a better signal-to-noise ratio. It is now possible to measure a meaningful spectrum within a fraction of an hour. This enables us to observe microscopic dynamics during hydrogen release in real time.

In this work, we will use neutron backscattering to monitor the reactions (1) and (2). Using the quasielastic amplitude as a proxy for the amount of Na<sub>3</sub>AlH<sub>6</sub> in the sample, we will show how this compound builds up in the first reaction step and disappears in the slower second step. Our results indicate that both reaction steps, after starting very slowly, are accelerated significantly when autocatalysis on the surface of Na<sub>3</sub>AlH<sub>6</sub> and NaH crystallites sets in. Preliminary data for TiCl<sub>3</sub>-doped NaAlH<sub>4</sub> suggest that the dopant acts like a nucleation center, accelerating the initial, non-autocatalytic phases of both reactions.

## II. SAMPLE PREPARATION

In this paper, we report on four sample materials: NaH, Na<sub>3</sub>AlH<sub>6</sub>, NaAlH<sub>4</sub>, and NaAlH<sub>4</sub>(a8a). All samples were prepared in an argon-filled glove box equipped with a recirculation system to keep the water and oxygen concentrations below 1 ppm. The raw chemicals NaH (95%, Sigma Aldrich), NaAlH<sub>4</sub> (96%, Albemarle), and TiCl<sub>3</sub> (99.999%, Sigma Aldrich) were used as received. Mechanical milling was carried out in a Fritsch P6 planetary mixer/mill at a rotation speed of 600 rpm using a silicon nitride vial and balls with a ball to powder weight ratio of about 20:1. The vial was filled and sealed in the glove box under argon atmosphere.

The samples were prepared as follows:

NaH: Powder as received.

Na<sub>3</sub>AlH<sub>6</sub>: Obtained by mechanical alloying of NaH and NaAlH<sub>4</sub> at a molar ratio of 2 to 1. The powder was milled for 20 h in an argon atmosphere as described in Refs. [6, 7]. The product was analyzed by X-ray diffraction

Pure NaAlH<sub>4</sub>: Powder as received, ball-milled for 30 minutes.

NaAlH<sub>4</sub> (a8a): Doped with TiCl<sub>3</sub>, cycled eight times under hydrogen, and quenched in the hydrogenated state. This sample was obtained by ball milling 2 g of NaAlH<sub>4</sub> and 285 mg of TiCl<sub>3</sub>, resulting in 5 mol.% Ti doping on the basis of TiCl<sub>3</sub>. In order to avoid any increase in the temperature, the 3 hours of milling were divided into 30 minutes of milling and 10 minutes pause with 5 repetitions. Directly after milling, the sample was first dehydrogenated, then cycled eight times under hydrogen with hydrogen absorption (100 °C, 100 bar) and desorption (150 °C, 0.3 bar) conditions, and finally quenched in the hydrogenated state. Absorption and desorption of hydrogen were carried out in a carefully calibrated modified Sieverts apparatus. A more detailed description of the apparatus, the reactor, and the absorption/desorption procedure can be found elsewhere [16, 32].

Unfortunately, lack of beamtime prevented us from measuring another doped sample, freshly prepared without hydrogen cycling.

The samples were filled into flat, top-loading  $30\times40\times0.5~\mathrm{mm^3}$  Al cells and sealed with Al wire in the glove box. In the course of this study, we were concerned about the sample material, while releasing hydrogen, possibly reacting with the cell. Therefore, we performed an additional measurement with NaAlH<sub>4</sub> powder filled into a pocket made of Ag foil to isolate the sample from the Al walls. Direct comparison of the neutron spectra revealed no difference.

## III. MEASUREMENTS AND DATA ANALYSIS

Since the samples are rich in hydrogen, the neutron scattering cross section is dominated by incoherent scattering by hydrogen.

Measurements were performed using the neutron backscattering spectrometer SPHERES of the Jülich Centre for Neutron Science (JCNS) at the neutron source FRM II (Forschungs-Neutronenquelle Heinz Maier-Leibnitz) in Garching, Germany [31]. To obtain reasonable statistics within short time slices we did not use the instrument's full energy range of  $\pm 31~\mu eV$ ; instead, the Doppler velocity amplitude was set to 1.3 m/s, giving access to a window of  $\pm 8.6~\mu eV$ .

The sample was mounted in a cryofurnace and oriented at 135°. In this standard geometry, self-shielding within the cell limits the range of useable scattering angles to  $2\theta \lesssim 125^\circ$ . This results in nine large-angle detectors with wavenumbers  $q=0.6\dots1.8~\text{Å}^{-1}$ . The small-angle detectors at  $q=0.25\dots0.46~\text{Å}^{-1}$  are not in exact backscattering and therefore have comparatively bad resolution.

The raw data reduction was carried out with SLAW [33], and further analysis was performed with FRIDA [34]. Spectra were normalized to the integral intensity at about room temperature. The room temperature measurements also served as resolution function.

Deviating from common practice, we did *not* subtract an empty-cell measurement. Instead, cell scattering was taken into account in the fitting procedure. In the energy range of SPHERES, scattering from Al just consists in a weak elastic line. Besides, there is a flat background due to various imperfections of the instrument. This background was determined from the baseline of the resolution spectrum, and included as a fixed component in all fit models. In fitting, squared deviations were weighed with the reciprocal standard deviation, and theoretical expressions are convoluted with the measured resolution function (minus the aforementioned baseline).

The data were analyzed in an heuristic and iterative way, trying different procedures and testing different models before a consistent overall picture emerged. In the following sections, data analysis will be decoupled from interpretation. In Sect. IV, spectral line shapes are analyzed, and simple fit functions are introduced. In Sect. V, fits are used to extract information from time-resolved measurements. Finally, in Sect. VI, the observations are interpreted physically.

## IV. SPECTRA

The simplest fit function that works for the entire data set is

$$S(q,\omega) = b + a_{\delta}\delta(\omega) + \sum_{i} a_{i}(q)\mathcal{L}(\omega, \Gamma_{i}).$$
 (3)

It consists of a flat background, an elastic  $\delta$  line, and zero, one, or two Lorentzians

$$\mathcal{L}(\omega; \Gamma) = \frac{1}{\pi} \frac{\Gamma}{\omega^2 + \Gamma^2}.$$
 (4)

The flat background is kept constant at the value determined at room temperature, except when the overall scattering decreases with time because of hydrogen desorption.

Unconstrained fits indicate that the Lorentzian linewidths do not vary systematically with q, whereas the amplitudes do. The amplitudes of the Lorentzians increase with q before they reach a plateau at about 1 Å<sup>-1</sup>. Therefore, in our final analysis of spectral lineshapes and time series, we average  $S(q,\omega)$  over the q range 0.9...1.8 Å<sup>-1</sup> to obtain a strong quasielastic signal with good statistics.

## A. NaH

Spectra of the final reaction product NaH were measured at 38, 117, and 177°C. In Fig. 1, these three spectra

have been rescaled to account for the temperature dependence of the elastic scattering (the Debye-Waller factor, or more precisely the Lamb-Mössbauer factor, since we are talking about self correlations measured by incoherent scattering). As a result, the spectra coincide perfectly, demonstrating the absence of quasielastic broadening.

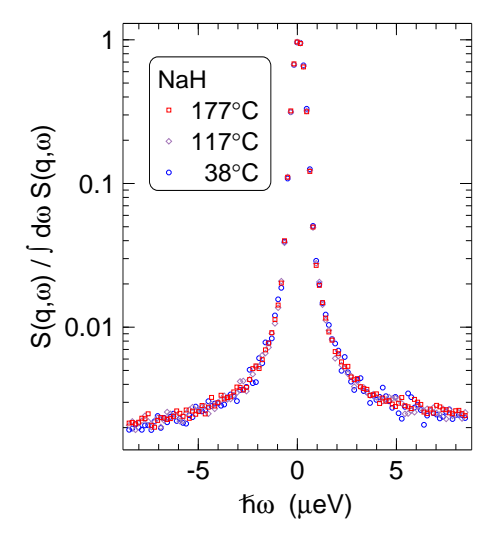


FIG. 1: Neutron scattering spectra of NaH measured using the backscattering spectrometer SPHERES. Here and in the following figures, spectral data are averaged over the q range  $0.9...1.8~{\rm \AA}^{-1}$ . Only in this figure, spectra are normalized to unit area to account for the temperature dependence of elastic scattering. There is no temperature-dependent quasielastic scattering; the spectra represent just the instrumental resolution function.

## B. Na<sub>3</sub>AlH<sub>6</sub>

The richest set of spectra was obtained for the intermediate reaction product Na<sub>3</sub>AlH<sub>6</sub>. Spectra of a freshly prepared sample were measured up to 177°C, where decomposition set in. Kinetic aspects will be discussed below (Sect. V).

Two Lorentzians are needed to describe the quasielastic scattering. To reduce the number of free parameters and to avoid unwanted degeneracies (discussed recently in another SPHERES data analysis [35]), amplitudes are fixed at temperature-independent values  $a_1 = 0.5$  and  $a_2 = 0.07$ . Excellent fits are obtained, as shown in Fig. 2.

To investigate the q dependence of the amplitudes  $a_{1,2}(q)$ , we impose the linewidths  $\Gamma_{1,2}(T)$  as determined from the fits to the q averaged spectra. Results are shown in Fig. 3. As anticipated, the  $a_{1,2}(q)$  are temperature-independent within experimental accuracy. Their q dependence is fitted reasonably well by the simple expression

$$a_{1,2}(q) = a_{1,2}^{\infty} \frac{q^2}{q^2 + \kappa^2}$$
 (5)

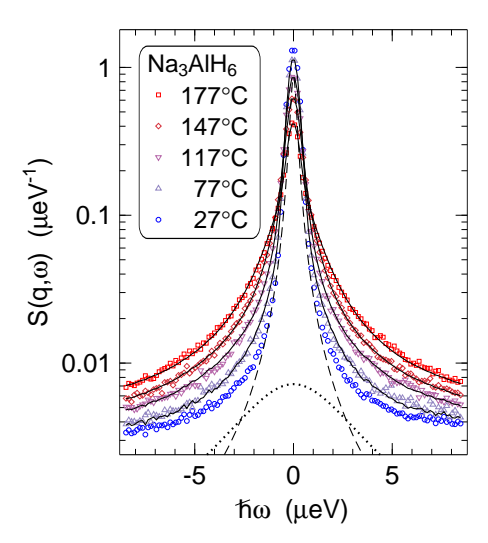


FIG. 2: Neutron scattering spectra of  $Na_3AlH_6$ . The  $27^{\circ}C$  data represent the resolution function. The other data are fitted according to Eq. (3) with a delta line and two Lorentzians (here and in the following figures, all spectral fits are understood to be convoluted with the measured resolution). The dashed (dotted) line shows the Lorentzian 1 (2) for  $117^{\circ}C$  separately and in unconvoluted form.

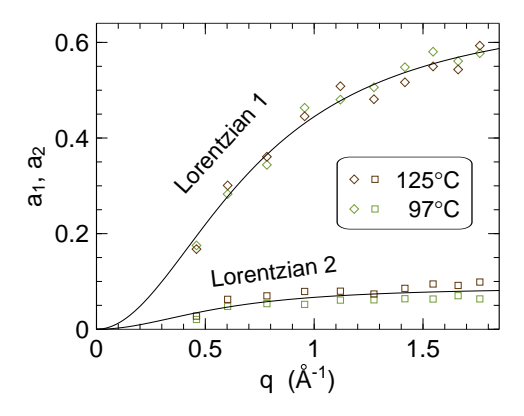


FIG. 3: Wavenumber dependence of the amplitudes  $a_{1,2}$  of the two Lorentzian components found when fitting the Na<sub>3</sub>AlH<sub>6</sub> spectra with Eq. (3). Solid lines: Fits with Eq. (5).

that interpolates between a  $q^2$  dependence for  $q \ll \kappa$  and a constant asymptote for  $q \gg \kappa$ .

Fig. 4 shows that the temperature dependence of the linewidths  $\Gamma_{1,2}(T)$  is compatible with an Arrhenius law  $\Gamma_i = \Gamma_i^0 \exp(-A_i/T)$ . The activation energies are  $A_1 = 38$  kJ/mol and  $A_2 = 23$  kJ/mol; the prefactors  $\Gamma_i^0$  are indicated in the figure. In estimating these parameters, some data points were excluded: linewidths below 0.1  $\mu$ eV were dropped, because they are too far below the instrumental resolution; data at 177°C had to be excluded, because the scattering signal was not stationary, so that the imposition of a fixed Lorentzian amplitude would not have been justified.

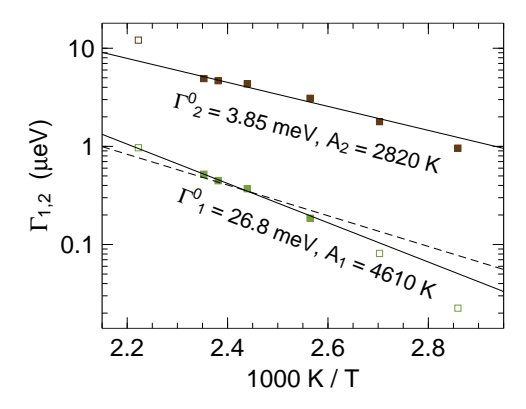


FIG. 4: Linewidths  $\Gamma_{1,2}(T)$  of the two Lorentzians used to fit the spectra of Na<sub>3</sub>AlH<sub>6</sub>. Only data shown as full symbols have been used to determine the Arrhenius laws shown as straight lines. The dashed line is obtained when proton NMR data [36] are taken into account (see Fig. 11;  $\Gamma_1^{0'}=2.3$  meV,  $A_1'=3600$  K).

## C. NaAlH $_4$

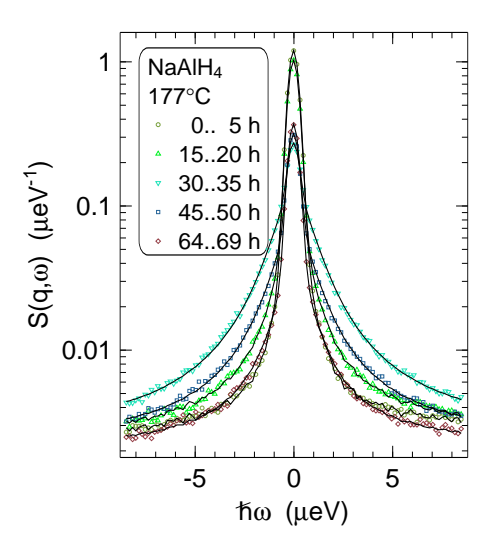


FIG. 5: Neutron scattering spectra of NaAlH $_4$  for various time intervals, after heating to 177°C.

Time-resolved measurements were performed with four fresh NaAlH<sub>4</sub> samples. After measuring the resolution at room temperature, the sample was quickly heated to 170, 180, or 185°C, and kept there at constant temperature for 2 days or more. Initially, no quasielastic scattering is observed. It takes several hours before a quasielastic signal appears above the wings of the resolution function. The signal continues to grow, until a maximum is reached about 30 h after the start of the measurement. Then, the quasielastic intensity decreases and about 65 h after the start of the measurement we are left with purely elastic scattering, which however is only half as strong as in the beginning.

To prepare for the detailed investigation of this kinet-

ics in Sect. V, we need to characterise the quasielastic lineshapes. To do so, the data are averaged over time slots of 5 h (Fig. 5). The minimal fit function that describes the entire data set consists of a flat background, a  $\delta$  line, and one Lorentzian. In contrast to the above analysis of Na<sub>3</sub>AlH<sub>6</sub>, the background must not be kept constant, because the total scattering intensity decreases during the experiment.

The Lorentzian linewidth at  $180^{\circ}$ C and for large q is about 1  $\mu$ eV. This is perfectly compatible with the Arrhenius law number 1 of Fig. 4. The slightly smaller and larger linewidths at 170 and  $185^{\circ}$ C are also compatible with this Arrhenius law. We therefore attribute the quasielastic scattering observed during the decomposition of NaAlH<sub>4</sub> entirely to the Lorentzian 1 that is dominant in Na<sub>3</sub>AlH<sub>6</sub>. In contrast, in the entire NaAlH<sub>4</sub> time series we find no trace of Lorentzian 2.

## D. NaAlH<sub>4</sub> (a8a)

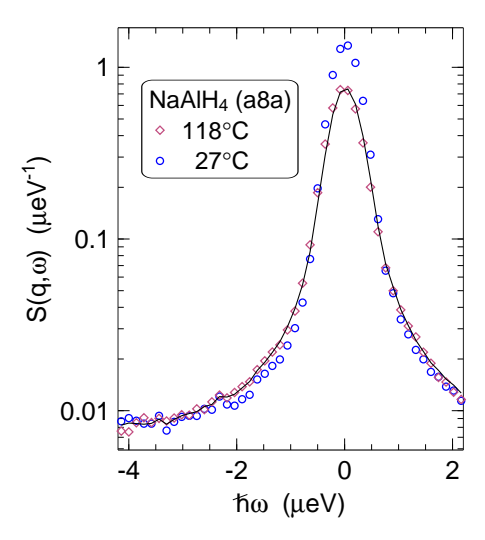


FIG. 6: Neutron scattering spectra of the TiCl<sub>3</sub>-doped NaAlH<sub>4</sub> (a8a) sample. A reduced  $\omega$  scale was chosen to emphasize the weak quasielastic scattering.

Due to a lack of beamtime, only one time-resolved measurement was performed with the TiCl<sub>3</sub>-doped NaAlH<sub>4</sub> (a8a) sample. After measuring the resolution at room temperature, the sample was heated in steps up to 118°C, where the onset of hydrogen release was noticed. During 20 h, the scattering intensity decayed by more than 50%. Before loosing the hydrogen completely, the temperature was increased to 131, 137, 167, 182°C for rather short measurements.

Fig. 6 shows the weak quasielastic scattering at 118°C. The fit consists of a free background, a  $\delta$  line, and a Lorentzian, with a fixed width of 0.20  $\mu$ eV derived from the Arrhenius description (Fig. 4) of Lorentzian 1 of the Na<sub>3</sub>AlH<sub>6</sub> analysis.

#### V. KINETICS

The results of the spectral analysis shall now be used for a quantitative description of the time-resolved measurements. Originally, one spectrum was saved every 5 minutes. In our analysis, we binned them into blocks of 20 min. While 20 min spectra are quite noisy, it is perfectly possible to perform a full spectral fit. The well-measured resolution function is taken into account just as in the last section. This fitting which can be completely automatized must, of course, not be construed as a model validation. But given a valid model, it is an efficient way of parameter extraction. The only condition is that fit parameters must not be close to degeneration. Therefore, it is of paramount importance that fixed Lorentzian linewidths as obtained from the Arrhenius laws of Fig. 4 are imposed.

## A. Na<sub>3</sub>AlH<sub>6</sub>

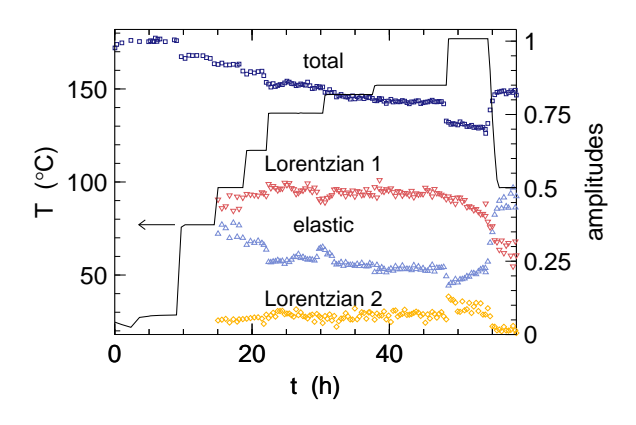


FIG. 7: Time-resolved backscattering measurement of  $Na_3AlH_6$ . Left scale: Experimental temperature sequence. Right scale: Total backscattering intensity, elastic intensity, and Lorentzian amplitudes.

Our time-resolved measurement of Na<sub>3</sub>AlH<sub>6</sub> is summarized in Fig. 7. The applied temperature sequence is shown along with the total backscattering intensity I (the integral of  $S(q,\omega)$  over the experimental energy range  $-8.6...8.6~\mu\text{eV}$ ) and the outcome of the fits, namely, the elastic intensity  $a_{\delta}$  and the two Lorentzian amplitudes  $a_{1.2}$ .

When heating step by step from room temperature to 152°C, I and  $a_{\delta}$  exhibit a parallel decrease: This is, at least qualitatively, the expected evolution of a Lamb-Mössbauer factor. Reliable amplitudes  $a_{1,2}$  can only be determined from 97°C onwards. In the range 97...152°C, both Lorentzian amplitudes are basically constant, which validates our fitting method with fixed linewidths  $\Gamma_{1,2}$ .

Shortly before heating to 147°C, there is a transient, complementary excursion in  $a_{\delta}$  and  $a_{1}$ , which we cannot explain. Another strange feature is the complementary

step in  $a_{\delta}$  and  $a_2$  after heating to 177°C. It is related to the outlier  $\Gamma_2(177^{\circ}\text{C})$  in Fig. 4, indicating a limitation of our fit.

We measured about 6 h at  $177^{\circ}$ C. During this time, the quasielastic amplitude  $a_1$  decreased by 0.14. This was partly compensated by an increase in elastic scattering of 0.05 so that the total backscattering decreased only by 0.06.

At this point, we decided not to wait for complete decomposition but to cool back to 117°C for comparison with spectra measured before the excursion to higher temperatures. Comparison revealed a decrease  $\Delta a_1 = -0.15$ ,  $\Delta a_2 = -0.03$ , partly compensated by an increase  $\Delta a_\delta = 0.10$ , resulting in a decrease of the total backscattering of  $\Delta I = -0.09$ .

## B. NaAlH<sub>4</sub>

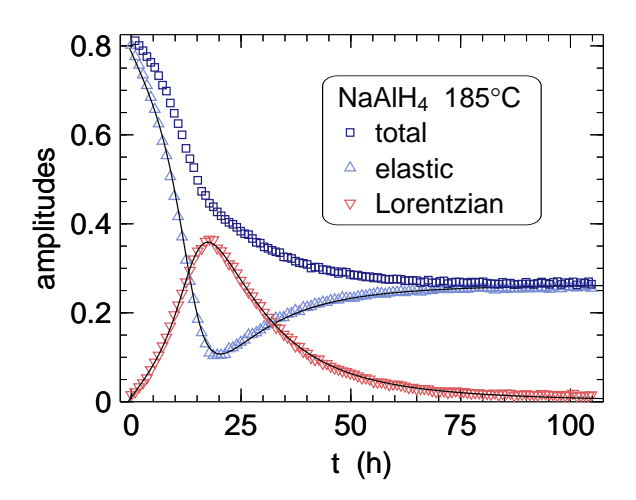


FIG. 8: Transformation of NaAlH<sub>4</sub> at 185°C: Total backscattering intensity I and fitted amplitudes  $a_{\delta}$  and  $a_{1}$  [Eq. (3)] versus time. Solid lines are fits with a kinetic model described in Sect. VI B.

As already shown in Fig. 5, quasielastic scattering slowly emerged after heating NaAlH<sub>4</sub> to a temperature in the range of 170...185°C, only to disappear some 10 h later. For a closer analysis, all 20 min spectra were fitted with a free background, a  $\delta$  line, and one Lorenztian of fixed width  $\Gamma_1(T)$  taken from the Arrhenius fit of Fig. 4.

Fig. 8 depicts the total backscattering intensity I and the amplitudes  $a_{\delta}$ ,  $a_{1}$  as function of time, along with a fit that will be discussed below in Sect. VI B. The quasielastic amplitude  $a_{1}$  reaches a maximum after about 18 h, before it decays slowly. In the long term, this decay is exponential, with a half life of about 10 h. The elastic intensity  $a_{\delta}$  decreases to less than 1/6 of its initial value, before recovering up to about 1/4 of the room temperature value. Total backscattering decreases continuously.

This time-resolved measurement was carried out four times at three different sample temperatures of 170, 180, and  $185^{\circ}$ C. Fig. 9 shows the time dependence of  $a_1$  for

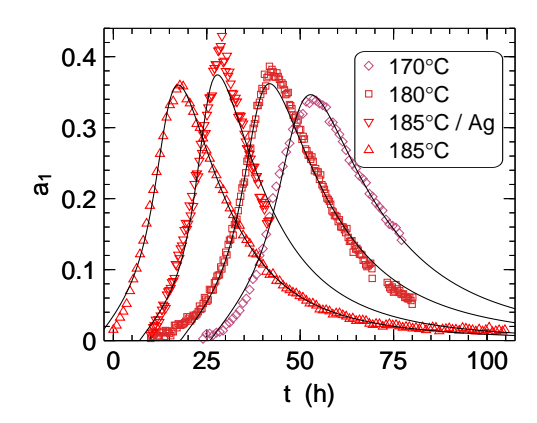


FIG. 9: Quasielastic amplitude  $a_1$  in four experiments on NaAlH<sub>4</sub> versus time. Time scales are arbitrarily shifted to keep the curves separated. "Ag" designates a sample that was isolated from its Al container by a silver foil. Solid lines are fits with the same kinetic model as in Fig. 8.

all four runs. With increasing temperature, the peaks are somewhat sharper; in particular, the initial slope is much steeper. There is some fluctuation in the maximum value of  $a_1$ , but altogether the curves demonstrate a very statisfactory reproducibility of measurements and data analysis.

## C. NaAlH<sub>4</sub> (a8a)

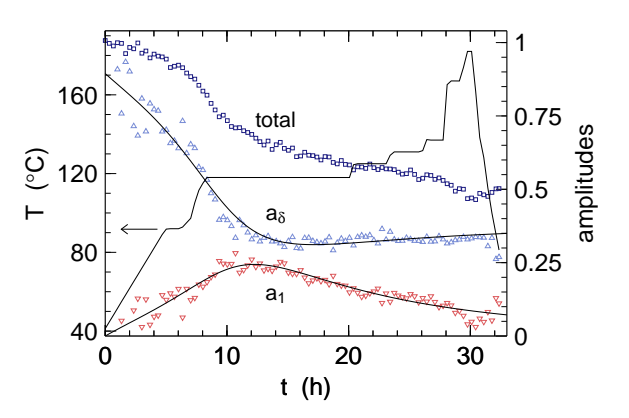


FIG. 10: Time-resolved backscattering measurement of TiCl<sub>3</sub>-doped NaAlH<sub>4</sub> (a8a). Left scale: Experimental temperature sequence. Right scale: Total backscattering intensity, elastic intensity, and Lorentzian amplitudes. Solid lines are fits with the same kinetic model as in Fig. 8, to be discussed in Sect. VIC.

For the TiCl<sub>3</sub>-doped NaAlH<sub>4</sub> (a8a) sample, we have so far undertaken one measurement only, with an improvized, unsystematic temperature sequence, as shown in Fig. 10. Quasielastic scattering seems to set in below 80°. However, fits at such low temperatures are not reliable, because the linewidth  $\Gamma_1(T)$  is far below the instrumental resolution. Once the sample is heated to 118°C, the quasielastic amplitude reaches its maximum within less than 2 h. Then, a slow decay sets in, with a half life of about 14 h. The temperature excursion to 167 and 182°C is accompanied by a dip in  $a_1$ : It is not clear whether this is physical; it depends critically on the Arrhenius fit used for imposing  $\Gamma_1(T)$ .

## VI. INTERPRETATION

#### A. Quasielastic Scattering by Na<sub>3</sub>AlH<sub>6</sub>

The Lorentzians used to fit the quasielastic scattering have temperature-independent amplitudes a(q) and wavenumber-independent linewidths  $\Gamma(T)$  in a good first approximation. This is the signature of localized processes. We see no scattering by long-ranged diffusion: Most probably, diffusion of  $H_2$  is too fast and diffusion of heavier species is too slow to be observed within the dynamic window of SPHERES.

Lorentzian 1 is due to internal motion of Na<sub>3</sub>AlH<sub>6</sub>: It is dominant in the quasielastic scattering of a freshly prepared sample, and found as a transient during the decomposition of NaAlH<sub>4</sub>, as expected from the two-step reaction formula (1), (2).

In contrast, Lorentzian 2 only is a small contribution to scattering of the fresh Na<sub>3</sub>AlH<sub>6</sub> sample; it is not visible during decomposition of NaAlH<sub>4</sub>. Its origin must be left unresolved.

The observed q dependence of the quasielastic amplitudes  $a_{1,2}$ , approximately described by Eq. (5), is not compatible with elementary jump models that would require an oscillatory q dependence  $a \propto [1 - j_0(dq)]$  (jump length  $\mathcal{O}(d)$ , spherical Bessel function  $j_0$ ) [37]. One possible explanation could be that each Lorentzian results from more than one internal mode, with similar frequencies, but different jump lengths so that (5) results as an average of  $1 - j_0(dq)$  over several d.

Rotational motion in Na<sub>3</sub>AlH<sub>6</sub> below room temperature was studied previously by NMR [36, 38]. Results indicated thermally activated rotational jumps of AlH<sub>6</sub> octahedra around  $C_4$  axes. Jump frequencies, described by Arrhenius laws, are indicated in Fig. 11. The slow  $C_{4XY}$  rotations of Ref. [36] were found to admit activation energies between 20 and 30 kJ/mol. Choosing the latter value, the Arrhenius law (the dashed line in Figs. 4 and 11) extrapolates quite well towards the linewidths of our Lorentzian 1. This further supports our interpretation of the Lorentzian 1 being due to internal rotations in Na<sub>3</sub>AlH<sub>6</sub>.

## B. Decomposition of NaAlH<sub>4</sub>

The increase and decrease of quasielastic scattering (Figs. 5, 8) reflect the production and consumption of Na<sub>3</sub>AlH<sub>6</sub> in the two-step reaction (1), (2), respectively.

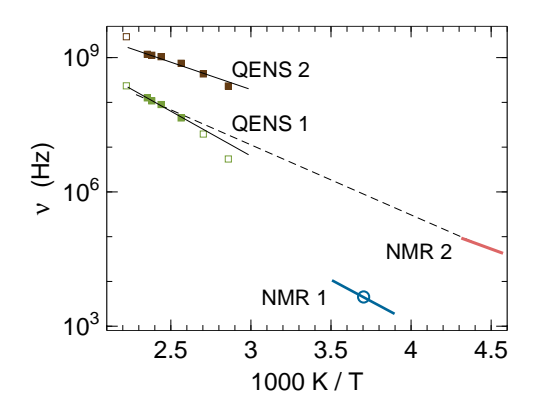


FIG. 11: Rotation frequencies in  $Na_3AlH_6$  as determined by quasielastic neutron scattering (QENS) and by nuclear magnetic responance (NMR). The QENS data are the same as in Fig. 4. The data point NMR 1 and the corresponding Arrhenius law was taken from [38]. The Arrhenius law NMR 2 is from [36]. The dashed line is the same as in Fig. 4; it suggests that NMR 2 and QENS 1 are one and the same process.

For better readability, we abbreviate these reaction equations as  $A \to B \to C$ , where A stands for NaAlH<sub>4</sub>, B for 1/3 Na<sub>3</sub>AlH<sub>6</sub>, and C for NaH. Side products of the reactions are not denoted, because they are irrelevant for the observed spectra: Al has a negligible neutron cross section, and H<sub>2</sub> leaves the sample so rapidly that it does not contribute to the scattering either.

Concentrations shall be written as dimensionless mol/mol fractions, normalized to a pure NaAlH<sub>4</sub> sample. Accordingly, the initial concentrations are [A] = 1, [B] = [C] = 0. Since our scattering signal is almost exclusively due to bound hydrogen, we set

$$a_1(t) = \frac{1}{2}[B]f_B,$$
 (6)

$$a_{\delta}(t) = [A]f_A + \frac{1}{4}[C]f_C,$$
 (7)

where the f are Lamb-Mössbauer factors.

On this base, we searched for rate equations that reproduce the observed time series  $a_1(t)$  and  $a_{\delta}(t)$ . We first used the code generator kinpy [39] to try kinetic models based on stochiometric reaction equations. It turned out that the relatively sharp peak in  $a_1(t)$  can only be reproduced if some autocatalysis is assumed. To improve the agreement with the experimental  $a_{\delta}(t)$  and  $a_1(t)$ , we admitted concentration dependences with fractional exponents. In this heuristic way, we found that the following kinetic model is about the simplest one that is compatible with the measured  $a_{\delta}(t)$  and  $a_1(t)$ :

$$d[A]/dt = -k_{00}[A] - k_{01}[A][B]^{2},$$

$$d[B]/dt = -d[A]/dt - d[C]/dt,$$

$$d[C]/dt = k_{10}[B]^{4/3} + k_{11}[B]^{4/3}[C]^{2/3},$$
(8)

At 185°C, the following rate coefficients are found:

$$k_{00} = 0.029 \,\mathrm{h}^{-1},$$
  
 $k_{01} = 0.55 \,\mathrm{h}^{-1},$   
 $k_{10} = 0.016 \,\mathrm{h}^{-1},$   
 $k_{11} = 0.097 \,\mathrm{h}^{-1}.$  (9)

The spontaneous rate coefficients  $k_{j0}$  (j = 0, 1) are smaller by about an order of magnitude than the autocatalytic ones  $k_{j1}$ , and the second autocatalytic step is much slower than the first one, as was to be expected from the shape of  $a_1(t)$ .

For the fits at different temperatures in Fig. 9, the spontaneous rates  $k_{j0}$  were fixed. Besides a trivial time shift, the only adjustable parameters were the two autocatalytic rates  $k_{j1}$ . Their fitted values show a plausible, weak temperature dependence. The fits are not perfect, but this does does not necessarily indicate a failure of our kinetic model; it could also point to the limits of experimental reproducibility (sample preparation, thermal history).

The exponents in (8) cannot be determined very accurately; it can only be said that they are compatible with multiples of 2/3, as expected for an autocatalytic reaction that takes place at a surface. We suggest that  $k_{j0}$  stands for nucleation and  $k_{j1}$  for crystallite growth.

Our model is perfectly compatible with the reaction pathways proposed in a density-functional study [40]. Based on first-principles calculations, the migrating species were suggested to be AlH<sub>3</sub> and NaH vacancies. The lowest activation energy was found for AlH<sub>3</sub> vacancies, leading to the following pathway for reaction (1):

$$n$$
NaAlH<sub>4</sub>  $\rightarrow n$ NaAlH<sub>4</sub><sup>AlH<sub>3</sub></sup> + Al +  $\frac{3}{2}$ H<sub>2</sub>, (10)

where the superscript denotes one vacancy, and n indicates an arbitrary amount of bulk material. The proposed diffusion mechanism also involves an  $AlH_5^{2-}$  ion. Anyway, the vacancy ultimately reaches a NaAlH<sub>4</sub>– Na<sub>3</sub>AlH<sub>6</sub> boundary, where it annihilates, releasing an excess Na<sup>+</sup> that aggregates with the growing Na<sub>3</sub>AlH<sub>6</sub> phase. From another computational study we learn that this growth additionally requires a two-step transformation  $AlH_4^- \rightarrow AlH_5^{2-} \rightarrow AlH_6^{3-}$  [24]. Coming back to Ref. [40], an alternate pathway starts

Coming back to Ref. [40], an alternate pathway starts with the unassisted release of Na<sup>+</sup> and H<sup>-</sup> at the boundary of the growing Na<sub>3</sub>AlH<sub>6</sub> according to

$$n$$
NaAlH<sub>4</sub>  $\rightarrow (n-1)$ NaAlH<sub>4</sub><sup>2NaH</sup> + Na<sub>3</sub>AlH<sub>6</sub>. (11)

The two ionic vacancies migrate together to the Al-NaAlH<sub>4</sub> boundary, where hydrogen is released:

$$n\text{NaAlH}_{4}^{\text{NaH}} \rightarrow (n-1)\text{NaAlH}_{4} + \text{Al} + \frac{3}{2}\text{H}_{2}.$$
 (12)

Using positron annilation, it was confirmed experimentally that vacancies are formed in NaAlH<sub>4</sub> during dehydrogenation [41].

In these pathways, boundaries play a crucial role: The NaAlH<sub>4</sub>-Na<sub>3</sub>AlH<sub>6</sub> boundary as a sink for AlH<sub>3</sub> vacancies

and as a source for NaH vacancies, and the Al–NaAlH $_4$  boundary as a sink for NaH vacancies and as the location of H $_2$  release. At least in undoped material, hydrogen release rates are limited by processes at these boundaries. This is in accordance with the autocatalytic terms of our kinetic model.

### C. Effect of Doping

In Fig. 10, the kinetic model (8) was applied to TiCl<sub>3</sub>-doped NaAlH<sub>4</sub>, cycled eight times under hydrogen and quenched in the hydrogenated state. These fits were at best a very rough first approximation, because constant rate coefficients were assumed although the sample temperature varied between 40 and 137°C (the excursion to 167...182°C was excluded from the fit). The model may even be entirely inappropriate, because the rate-limiting processes in doped alanate could be qualitatively different from those in pure material. According to [40], hydrogen release in pure material is limited by surface processes, whereas in doped material rates are determined by vacancy diffusion.

Under these reservation, the coefficients are about

$$k_{00} = 0.05 \text{ h}^{-1},$$
  
 $k_{01} = 0.8 \text{ h}^{-1},$   
 $k_{10} = 0.12 \text{ h}^{-1};$ 
(13)

 $k_{11}$  had no noticeable influence upon the time dependence of  $a_{\delta}(t)$  and  $a_{1}(t)$ . All three values in (13) are higher than their counterparts in (9) although the latter were determined at the considerably higher temperature of 170°C. Doping was expected to increase the coefficient  $k_{00}$ , so that the first decomposition step starts at much lower temperatures than in the undoped material. However, the effect of doping on the second decomposition step seems to be even stronger: The coefficient  $k_{10}$  is larger than in the undoped 185°C data by a full order of magnitude. This correlates with the observation that the peak height of  $a_{1}(t)$  is much lower in the doped than in the undoped material.

## VII. CONCLUSION

The high flux, low background, and fine resolution of the new backscattering spectrometer SPHERES opens up new perspectives for time-resolved studies of weak and narrow quasielastic spectra. The present work reveals the potential of this method for investigations of reaction kinetics.

The desorption of hydrogen from sodium alanate is an almost perfect test case, because on the one hand with its five different reactants it is complex enough to be interesting, while on the other hand the neutron spectra are not too complex, because two of the reactants do not noticeably contribute to the scattering, and only one of

them, the intermediate reaction product  $Na_3AlH_6$ , shows quasielastic scattering. Once these quasielastic spectra are well characterized, the time-resolved measurements allow for an automatic data reduction that yields a small number of time-dependent amplitudes. These amplitudes can be related in a straightforward way [Eqs. (6), (7)] to reactant concentrations.

A time-resolved measurement of NaAlH<sub>4</sub> decomposition at 170...185°C was fitted by a physically meaningful set of reaction rate equations. According to this model, both desorption steps (1), (2) are controlled by nucleation and growth.

Next, it will be interesting to investigate more systematically the temperature dependence of reaction rates. To initiate the decomposition of NaAlH<sub>4</sub>, there seems to be only a small temperature range between about  $165^{\circ}$ C and the melting point. However, once the reaction has started, its autocatalytic sequel possibly remains active at considerably lower temperatures.

While special care was taken to produce all samples in the same manner, it would be interesting to investigate how the kinetics depends on the initial texture and on the hydrogen loading/unloading prehistory.

Most importantly, the basis is now available for systematically investigating how the single reaction steps are modified by the presence of a dopant. As a very preliminary result, we hypothize that TiCl<sub>3</sub> mainly accelerates the spontaneous decomposition of the intermediate reactant Na<sub>3</sub>AlH<sub>6</sub>. However, this still needs thorough verification. Unfortunately, only a very narrow quasielastic signal can be observed at the low reaction temperatures made possible by doping (Fig. 6). Nevertheless, Fig. 10 suggests that a quantitative study of reaction kinetics will be possible if more systematic time runs will be measured.

## VIII. ACKNOWLEDGEMENTS

We thank Dr. Maximilian Fichtner for giving us the possibility to use the energy storage laboratory equipment for the preparation of the samples.

- Schüth F, Bogdanović B and Felderhoff M (2004) Chem. Comm. 2249.
- [2] Orimo S-i, Nakamori Y, Eliseo J R, Züttel A and Jensen C M (2007) Chem. Rev. 107 4111.
- [3] Eberle U, Felderhoff M. and Schüth F (2009) Angew. Chem. Int. Ed. 48 6608.
- [4] Bogdanović B and Schwickardi M (1997) J. Alloys Comp. 253–254 71.
- [5] Anton D L (2003) J. Alloys Comp. **356–357** 400.
- [6] Zaluski L, Zaluska A and Ström-Ölsen J O (1999) J. Alloys Comp. 290 71.
- [7] Huot J, Boily S, Güther V and Schulz R (1999) J. Alloys Comp. 283 304.
- [8] Kang X-D, Wang P and Cheng H-M (2007) J. Phys. Chem. C 111 4879.
- [9] Bogdanović B, Brand R A, Marjanović A, Schwickardi M and Tölle J (2000) J. Alloys Comp. 302 36.
- [10] Luo W and Gross K J (2004) J. Alloys Comp. 385 224.
- [11] Lee B-M, Jang J-W, Shim J-H, Cho Y W and Lee B-J (2006) J. Alloys Comp. 424 370.
- [12] Mueller T and Ceder G (2010) ACS Nano 4 5647.
- [13] Singh S, Eijt S W H, Huot J, Kockelmann W A, Wage-maker M and Mulder F M (2007) Acta Mater. 55 5549.
- [14] Claudy P, Bonnetot B, Chahine G and Letoffe J M (1980) Thermochim. Acta 38 75.
- [15] Jensen C M and Gross K J (2001) Appl. Phys. A 72 213.
- [16] Kircher O and Fichtner M (2004) J. Appl. Phys. 95 7748.
- [17] Felderhoff M, Klementiev K, Grünert W, Spliethoff B, Tesche B, Bellosta von Colbe J M, Bogdanović B, Härtel M, Pommerin A, Schüth F and Weidenthaler C (2004) Phys. Chem. Chem. Phys. 6 4369.
- [18] Kiyobayashi T, Srinivasan S S, Sun D and Jensen C M (2003) J. Phys. Chem. A 107 7671.
- [19] Fichtner M, Canton P, Kircher O and Léon A (2005) J. Alloys Comp. 404–406 732.

- [20] Bellosta von Colbe J M, Schmidt W, Felderhoff M, Bogdanović B and Schüth F (2006) Angew. Chem. Int. Ed. 45 3663.
- [21] Lohstroh W and Fichtner M (2007) Phys. Rev. B 75 184106.
- [22] Chaudhuri S and Muckerman J T (2005) J. Phys. Chem. B 109 6952.
- [23] Vegge T (2006) Phys. Chem. Chem. Phys. 8 4853.
- [24] Dathar G K P and Mainardi D S (2010) J. Phys. Chem. C 114 8026.
- [25] Sun D, Kiyobayashi T, Takeshita H T, Kuriyama N and Jensen C M (2002) J. Alloys Comp. 337 L8.
- [26] Moysés Araújo C, Li S, Ahuja R and Jena P (2005) Phys. Rev. B 72 165101.
- [27] Bai K and Wu P (2006) Appl. Phys. Lett. 89 201904.
- [28] Andreasen A, Hjøllum J, Vegge T, Engberg D, Niedermayer C and Lefmann K Sing experimental report, http://sinq.web.spi.ch/sinq/er/ii\_04r\_10.pdf, last change 11-apr-2005, retrieved 27-sep-2010.
- [29] Shi Q, Voss J, Jacobsen H S, Lefmann K, Zamponi M and Vegge T (2007) J. Alloys Comp. 446–447 469.
- [30] Voss J, Shi Q, Jacobsen H S, Zamponi M, Lefmann K and Vegge T (2007) J. Phys. Chem. B 111 3886.
- [31] Wuttke J et al. Spheres online manual, http://www.jcns.info/jcns\_spheres.
- [32] Fichtner M, Fuhr O, Kircher O and Rothe J (2003) Nanotechnology 14 778.
- [33] Wuttke J Slaw: neutron scattering histograms to scattering law converter, http://www.messen-und-deuten.de/slaw.
- [34] Wuttke J Frida: Flexible rapid interactive data analysis, http://www.messen-und-deuten.de/frida.
- [35] Doster W, Busch S, Gaspar A M, Appavou M S, Wuttke J and Scheer H (2010) Phys. Rev. Lett. 104 098101.
- [36] Verkuijlen M H W, van Bentum P J M, van Eck E R H,

- Lohstroh W, Fichtner M and Kentgens A P M (2009)  $J.\ Phys.\ Chem.\ C$  113 15467.
- [37] Bée M (1985) Quasielastic Neutron Scattering, Adam Hilger: Bristol (1985).
- [38] Senegas J, Villepastour A M and Bonnetot B (1981) J. Phys. Chem. Solids 42 1061.
- [39] Srinivasan A kinpy: a source code generator
- for solving chemical kinetic equations in python, http://code.google.com/p/kinpy/.
- [40] Gunaydin H, Houk K N and Ozolinš V (2008) Proc. Natl. Acad. Sci. USA 105 3673.
- [41] Sakaki K, Nakamura Y, Akiba E, Kuba M T and Jensen C M (2010) J. Phys. Chem. C  $\bf 114$  6869.